

Prompt Fission Neutron Uranium Logging(III): Logging Instrument*

Hai-Tao Wang ^{§,1,2} Yan Zhang ^{§,1,2,†} Chi Liu, ^{1,2} Jian-Qiang Xu, ^{1,2} Li-Jiao Zhang, ^{1,2} Zhi-Feng Liu, ^{1,2}
Xiong-Jie Zhang, ^{1,2} Rui Chen, ^{1,2} Qi Liu, ^{1,2} Ren-Bo Wang, ^{1,2} Shu-Min Zhou, ^{1,2} and Bin Tang ^{1,2}

¹*National Key Laboratory of Uranium Resources Exploration-Mining and Nuclear Remote Sensing,
East China University of Technology, Nanchang, 330000, China*

²*Engineering Research Center of Nuclear technology Application,
Ministry of Education, East China University of Technology, Nanchang, 330013, China*

The domestically developed prompt fission neutron uranium logging(PFNUL) instrument for uranium exploration represents a significant advancement in China deep uranium mining efforts, though it comes with considerable challenges and complexity. This paper presents the development of a new prompt fission neutron uranium logging instrument(named UNL4) , integrates a domestic D-T neutron generator, two ³He proportional detectors, a lanthanum bromide (LaBr₃) gamma-ray detector, and digital multi-channel pulse amplitude analyzer. The near ³He detector is shielded with 1mm of Cadmium (Cd) and 5mm of high-density polyethylene(HDPE), enabling efficient epithermal neutron detection, while the far ³He detector measures thermal neutron. The LaBr₃ detector is employed for gamma-ray detection, primarily originating from uranium decay. High-speed ADC and FPGA technologies were used to achieve rapid acquisition and transmission of both dual neutron time spectra and gamma spectra.Moreover, this paper proposes a fast signal shaping method, which reduces the dead time effect in ³He detectors on neutron time spectra. Experiments conducted in standard model boreholes with varying uranium content demonstrated a strong linear relationship between the epithermal-to-thermal neutron ratio (E/T) and uranium content, with a fitting coefficient of $R^2>0.999$, confirming the instruments accuracy. The E/T value repeatability, both in short-term (3.16% RSD) and long-term (1.2% RSD) measurements, showed excellent stability. In addition, the instrument demonstrated good performance at neutron logging speeds of 0.3~3 m/min (E/T values) and gamma logging speeds of 1~10 m/min. By conducting measurements in two ore sections of the PU model with lithium contents of 87.1 ppm and 45.6 ppm, the RD is less than about 10% in both logging cases, meeting the requirements for engineering applications. This marks the first successful development of a neutron logging instrument for uranium exploration based on a domestic neutron generator, signifying an important contribution to uranium resource exploration.

Keywords: Uranium exploration; Neutron logging instrument; Pulsed neutron; Neutron time spectrum detection

I. INTRODUCTION

Nuclear power is one of the most promising methods for efficiently and sustainably producing hydrogen on a large scale without emitting carbon dioxide. Uranium ore, as the primary source of fuel for nuclear energy generation, is crucial for the development of the nuclear power industry. Since the beginning of the 21st century, countries around the world have initiated mineral exploration efforts and developed intelligent technologies and equipment for mineral exploration and development, providing technological support for energy conservation and emission reduction[1–4].

The uranium logging method based on pulsed neutron technology allows for the direct measurement of uranium (²³⁵U) content without the need for core sampling, and it is not affected by the gamma rays from other radioactive nuclides

such as thorium and potassium [5–7]. Since the 1970s, countries including the United States, Canada, Germany, and the former Soviet Union have conducted research and experiments on neutron logging techniques for direct uranium measurement. It is widely recognized that collecting neutron time spectra is an effective method for quantifying uranium [8–10]. However, it is essential to utilize neutron sources with ultra-short pulse widths and high yields, such as the pulsed neutron uranium logging system ANHK-60 developed by the Russian All-Russian Institute of Automated Design (VNIIA), which employs a D-T neutron generator with a pulse width of 1 μ s and a single pulse yield of approximately 10^8 n/pulse, but its operational lifespan is limited to only 150 hours [11, 12].

In recent years, research on neutron logging has primarily focused on methods, theory, and simulation studies, with fewer reports on related instruments [13, 14]. This is largely due to the significant challenges involved in developing uranium logging instruments. One key requirement is the use of compact neutron emitters that produce ultra-short pulses (on the order of microseconds) with high neutron yields. Currently, only a few countries, including Russia, the United States, and France have developed such technology. Examples include Russia ING-10-20-120 model D-T neutron emitter, France Genie 16NG, and the U.S. RTNS-II and P383 systems [15–17]. Another challenge is detecting and collecting the neutron signals generated by these short-pulse, high-yield neutron sources. The widely adopted approach is to use high-

[§] These authors contributed equally to this work

* Supported by the National Natural Science Foundation of China (NO. 42374226), Jiangxi Provincial Natural Science Foundation (NO. 20232BAB201043 and 20232BCJ23006), National Key Laboratory of Uranium Resource Exploration-Mining and Nuclear Remote Sensing(2024QZ-TD-09), nuclear energy development project (20201192-01) and Young Talent Support Project of ECUT(DHTJBJ202402)

† Corresponding author, Yan Zhang, yanzhang@ecut.edu.cn.

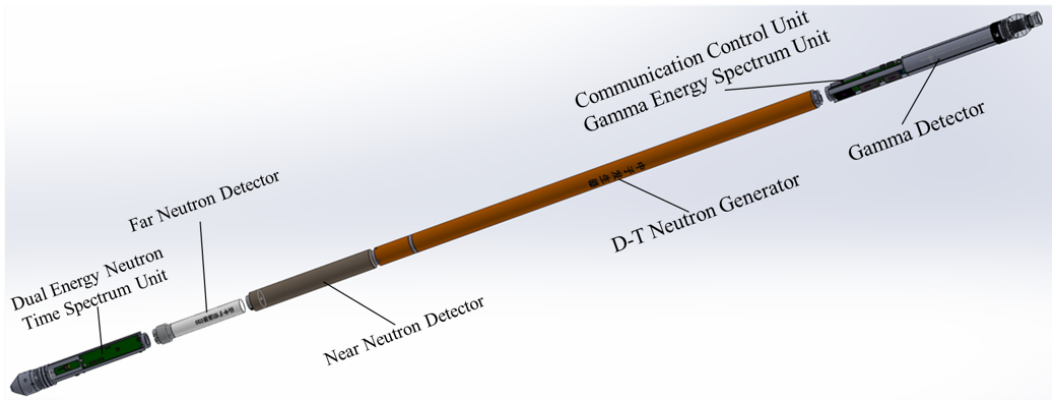


Fig. 1. Independently developed Prompt Fission Neutron Uranium Logging Instrument(UNL4)

43 efficiency ^3He proportional counters to detect epithermal or
 44 thermal neutrons. Epithermal neutron detectors are used to
 45 detect prompt neutrons produced by uranium fission, which
 46 are essential for uranium quantification [18]. For example,
 47 the Russian ANHK-60 logging instrument includes six GM
 48 tubes to detect gamma rays from lead and boron, forming a
 49 monitoring system for neutron source yield, thus mitigating
 50 the impact of source flux fluctuations. The U.S. PFN sys-
 51 tem is equipped with six miniature ^3He proportional counters
 52 to achieve similar functionality [19]. In the past decade, the
 53 author team has conducted extensive research in the field of
 54 neutron logging for uranium. Through both theoretical and
 55 experimental work, they proposed a method based on the ra-
 56 tio of epithermal neutrons(E) to thermal neutrons(T), referred
 57 to as "E/T" [20–23]. This method is not affected by fluctu-
 58 ations in the neutron source yield, allowing for an extended
 59 operational lifespan of the neutron source [24]. Therefore, the
 60 uranium logging instrument discussed in this paper utilizes
 61 two ^3He proportional counters. The first, located closer to the
 62 source, is wrapped in cadmium and high-density polyethy-
 63 lene for epithermal neutron detection, while the second, far-
 64 ther from the source, detects thermal neutrons [25–27]. How-
 65 ever, factors such as gas pressure and the material and size
 66 of the wrapping layers significantly affect neutron detection
 67 efficiency, which is a key topic of this study. Given that the
 68 smallest exploration boreholes are only 9 cm in diameter, ex-
 69 isting commercial multi-channel analyzers for time and en-
 70 ergy spectra do not meet the size requirements for logging
 71 instruments, and the large data volumes generated require re-
 72 design and customization. This paper proposes using high-
 73 speed ADC and FPGA technology to enable rapid acquisition
 74 and transmission of dual neutron time spectra, combined with
 75 pulse shaping techniques and time spectrum processing algo-
 76 rithms, to meet the specific needs of logging instrumentation
 77 [28].

78 Finally, a series of experiments were conducted using the
 79 independently developed prompt fission neutron uranium log-
 80 ging instrument(UNL4) in five standard model boreholes at
 81 the Nuclear Industry Airborne Survey and Remote Sensing
 82 Center. The calibration results from these model boreholes
 83 with varying uranium concentrations demonstrated a strong

84 linear relationship in the uranium content calibration equa-
 85 tion, comparable to that obtained using the probe equipped
 86 with the Russian neutron tube. The instrument also per-
 87 formed well in both short-term and long-term repeatability
 88 tests conducted in the same model boreholes, ensuring ac-
 89 curate calibration of uranium content. A comparison of log-
 90 ging curves at different speeds indicates that the measurement
 91 performance is satisfactory at neutron logging speeds ranging
 92 from 0.3 to 3 m/min and gamma logging speeds from 1 to
 93 10 m/min. This instrument fills a critical gap in the indepen-
 94 dent development of neutron logging instruments for uranium
 95 exploration in China and holds significant importance for ura-
 96 nium resource exploration and the country energy security.

97 II. INSTRUMENTS AND EXPERIMENTS

98 A. Logging Instrument

99 The uranium logging instrument developed by our team,
 100 as shown in Fig. 1, comprises three main components: (1)
 101 neutron source: including a D-T neutron tube and neutron
 102 emitter; (2) detection unit: featuring two ^3He neutron detec-
 103 tors and a gamma detector; (3) electronics unit: consisting of
 104 digital multi-channel pulse amplitude analyzer.

105 The D-T neutron sources used in the experiments primarily
 106 include the Russian ING-10-20-120 model and the FH-G5DT
 107 model from Fan-Hua Testing Technology Co., Ltd., with de-
 108 tailed parameters listed in Table 1. These sources are mainly
 109 used for emitting pulsed neutrons. The ^3He neutron detectors,
 110 also provided by Fan-Hua Testing Technology Co., Ltd., are
 111 referred to as the near ^3He detector and the far ^3He detector,
 112 based on their proximity to the neutron source. The near ^3He
 113 detector is wrapped in cadmium (Cd) metal and high-density
 114 polyethylene is designed to detect epithermal neutrons, while
 115 the far ^3He detector is used for detecting thermal neutrons in
 116 the borehole. The gamma detector employed is a lanthanum
 117 bromide (LaBr_3) detector, positioned at a greater distance
 118 from the neutron source to minimize the effects of gamma
 119 rays produced by neutron activation. The primary function
 120 of the LaBr_3 detector is to detect the natural gamma radia-

tion emitted by uranium ore, providing an initial estimate of the ore layers location [29]. The electronics unit consists of time spectrum and energy spectrum acquisition components. It utilizes a fully digital design, incorporating high-speed A/D conversion, FPGA, and DSP technology. This setup enables high-speed sampling of neutron and gamma ray signals and intelligent processing of dual-energy neutron time spectra and gamma energy spectra. The system can operate both independently and in coordinated synchronization, offering enhanced performance. Further details are provided in the following sections.

Table 1. D-T neutron generator parameters

Neutron tube	ING-10-20-120	FH-G5DT
Neutron yield	1.5×10^8 n/s	1×10^8 n/s
Pulse frequency	1~20 Hz	0~1k Hz
Life	150 h	≥ 500 h
Supply Voltage	+150V(DC)	220V(AC/50Hz) /48V~260V(DC)
Maximum power	30 W	50 W
Maximum working temperature	+120°C	+150°C
Sizes	$\Phi 34\text{mm} \times 1300\text{mm}$	$\Phi 50\text{mm} \times 1300\text{mm}$

B. Epithermal and Thermal Neutron Detection

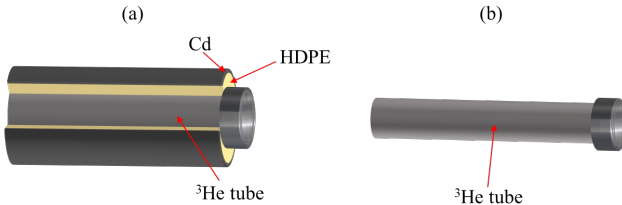


Fig. 2. (a) Schematic diagram of the Epithermal neutron detector (b) Schematic diagram of the Thermal neutron detector

$\frac{1}{2}$ $\frac{3}{4}$ $\frac{5}{6}$ $\frac{7}{8}$ $\frac{9}{10}$ $\frac{11}{12}$ $\frac{13}{14}$ $\frac{15}{16}$ $\frac{17}{18}$ $\frac{19}{20}$ $\frac{21}{22}$ $\frac{23}{24}$ $\frac{25}{26}$ $\frac{27}{28}$ $\frac{29}{30}$ $\frac{31}{32}$ $\frac{33}{34}$ $\frac{35}{36}$ $\frac{37}{38}$ $\frac{39}{40}$ $\frac{41}{42}$ $\frac{43}{44}$ $\frac{45}{46}$ $\frac{47}{48}$ $\frac{49}{50}$ $\frac{51}{52}$ $\frac{53}{54}$ $\frac{55}{56}$ $\frac{57}{58}$ $\frac{59}{60}$ $\frac{61}{62}$ $\frac{63}{64}$ $\frac{65}{66}$ $\frac{67}{68}$ $\frac{69}{70}$ $\frac{71}{72}$ $\frac{73}{74}$ $\frac{75}{76}$ $\frac{77}{78}$ $\frac{79}{80}$ $\frac{81}{82}$ $\frac{83}{84}$ $\frac{85}{86}$ $\frac{87}{88}$ $\frac{89}{90}$ $\frac{91}{92}$ $\frac{93}{94}$ $\frac{95}{96}$ $\frac{97}{98}$ $\frac{99}{100}$ $\frac{101}{102}$ $\frac{103}{104}$ $\frac{105}{106}$ $\frac{107}{108}$ $\frac{109}{110}$ $\frac{111}{112}$ $\frac{113}{114}$ $\frac{115}{116}$ $\frac{117}{118}$ $\frac{119}{120}$ $\frac{121}{122}$ $\frac{123}{124}$ $\frac{125}{126}$ $\frac{127}{128}$ $\frac{129}{130}$ $\frac{131}{132}$ $\frac{133}{134}$ $\frac{135}{136}$ $\frac{137}{138}$ $\frac{139}{140}$ $\frac{141}{142}$ $\frac{143}{144}$ $\frac{145}{146}$ $\frac{147}{148}$ $\frac{149}{150}$ $\frac{151}{152}$ $\frac{153}{154}$ $\frac{155}{156}$ $\frac{157}{158}$ $\frac{159}{160}$ $\frac{161}{162}$ $\frac{163}{164}$ $\frac{165}{166}$ $\frac{167}{168}$ $\frac{169}{170}$ $\frac{171}{172}$ $\frac{173}{174}$ $\frac{175}{176}$ $\frac{177}{178}$ $\frac{179}{180}$ $\frac{181}{182}$ $\frac{183}{184}$ $\frac{185}{186}$ $\frac{187}{188}$ $\frac{189}{190}$ $\frac{191}{192}$ $\frac{193}{194}$ $\frac{195}{196}$ $\frac{197}{198}$ $\frac{199}{200}$ $\frac{201}{202}$ $\frac{203}{204}$ $\frac{205}{206}$ $\frac{207}{208}$ $\frac{209}{210}$ $\frac{211}{212}$ $\frac{213}{214}$ $\frac{215}{216}$ $\frac{217}{218}$ $\frac{219}{220}$ $\frac{221}{222}$ $\frac{223}{224}$ $\frac{225}{226}$ $\frac{227}{228}$ $\frac{229}{230}$ $\frac{231}{232}$ $\frac{233}{234}$ $\frac{235}{236}$ $\frac{237}{238}$ $\frac{239}{240}$ $\frac{241}{242}$ $\frac{243}{244}$ $\frac{245}{246}$ $\frac{247}{248}$ $\frac{249}{250}$ $\frac{251}{252}$ $\frac{253}{254}$ $\frac{255}{256}$ $\frac{257}{258}$ $\frac{259}{260}$ $\frac{261}{262}$ $\frac{263}{264}$ $\frac{265}{266}$ $\frac{267}{268}$ $\frac{269}{270}$ $\frac{271}{272}$ $\frac{273}{274}$ $\frac{275}{276}$ $\frac{277}{278}$ $\frac{279}{280}$ $\frac{281}{282}$ $\frac{283}{284}$ $\frac{285}{286}$ $\frac{287}{288}$ $\frac{289}{290}$ $\frac{291}{292}$ $\frac{293}{294}$ $\frac{295}{296}$ $\frac{297}{298}$ $\frac{299}{300}$ $\frac{301}{302}$ $\frac{303}{304}$ $\frac{305}{306}$ $\frac{307}{308}$ $\frac{309}{310}$ $\frac{311}{312}$ $\frac{313}{314}$ $\frac{315}{316}$ $\frac{317}{318}$ $\frac{319}{320}$ $\frac{321}{322}$ $\frac{323}{324}$ $\frac{325}{326}$ $\frac{327}{328}$ $\frac{329}{330}$ $\frac{331}{332}$ $\frac{333}{334}$ $\frac{335}{336}$ $\frac{337}{338}$ $\frac{339}{340}$ $\frac{341}{342}$ $\frac{343}{344}$ $\frac{345}{346}$ $\frac{347}{348}$ $\frac{349}{350}$ $\frac{351}{352}$ $\frac{353}{354}$ $\frac{355}{356}$ $\frac{357}{358}$ $\frac{359}{360}$ $\frac{361}{362}$ $\frac{363}{364}$ $\frac{365}{366}$ $\frac{367}{368}$ $\frac{369}{369}$ $\frac{371}{372}$ $\frac{373}{374}$ $\frac{375}{376}$ $\frac{377}{378}$ $\frac{379}{379}$ $\frac{381}{382}$ $\frac{383}{384}$ $\frac{385}{386}$ $\frac{387}{388}$ $\frac{389}{389}$ $\frac{391}{392}$ $\frac{393}{394}$ $\frac{395}{395}$ $\frac{397}{398}$ $\frac{399}{399}$ $\frac{401}{402}$ $\frac{403}{404}$ $\frac{405}{406}$ $\frac{407}{408}$ $\frac{409}{409}$ $\frac{411}{412}$ $\frac{413}{414}$ $\frac{415}{416}$ $\frac{417}{418}$ $\frac{419}{419}$ $\frac{421}{422}$ $\frac{423}{424}$ $\frac{425}{426}$ $\frac{427}{428}$ $\frac{429}{429}$ $\frac{431}{432}$ $\frac{433}{434}$ $\frac{435}{436}$ $\frac{437}{438}$ $\frac{439}{439}$ $\frac{441}{442}$ $\frac{443}{444}$ $\frac{445}{446}$ $\frac{447}{448}$ $\frac{449}{449}$ $\frac{451}{452}$ $\frac{453}{454}$ $\frac{455}{456}$ $\frac{457}{458}$ $\frac{459}{459}$ $\frac{461}{462}$ $\frac{463}{464}$ $\frac{465}{466}$ $\frac{467}{468}$ $\frac{469}{469}$ $\frac{471}{472}$ $\frac{473}{474}$ $\frac{475}{476}$ $\frac{477}{478}$ $\frac{479}{479}$ $\frac{481}{482}$ $\frac{483}{484}$ $\frac{485}{486}$ $\frac{487}{488}$ $\frac{489}{489}$ $\frac{491}{492}$ $\frac{493}{494}$ $\frac{495}{495}$ $\frac{497}{498}$ $\frac{499}{499}$ $\frac{501}{502}$ $\frac{503}{504}$ $\frac{505}{506}$ $\frac{507}{508}$ $\frac{509}{509}$ $\frac{511}{512}$ $\frac{513}{514}$ $\frac{515}{516}$ $\frac{517}{518}$ $\frac{519}{519}$ $\frac{521}{522}$ $\frac{523}{524}$ $\frac{525}{526}$ $\frac{527}{528}$ $\frac{529}{529}$ $\frac{531}{532}$ $\frac{533}{534}$ $\frac{535}{536}$ $\frac{537}{538}$ $\frac{539}{539}$ $\frac{541}{542}$ $\frac{543}{544}$ $\frac{545}{546}$ $\frac{547}{548}$ $\frac{549}{549}$ $\frac{551}{552}$ $\frac{553}{554}$ $\frac{555}{556}$ $\frac{557}{558}$ $\frac{559}{559}$ $\frac{561}{562}$ $\frac{563}{564}$ $\frac{565}{566}$ $\frac{567}{568}$ $\frac{569}{569}$ $\frac{571}{572}$ $\frac{573}{574}$ $\frac{575}{576}$ $\frac{577}{578}$ $\frac{579}{579}$ $\frac{581}{582}$ $\frac{583}{584}$ $\frac{585}{586}$ $\frac{587}{588}$ $\frac{589}{589}$ $\frac{591}{592}$ $\frac{593}{594}$ $\frac{595}{595}$ $\frac{597}{598}$ $\frac{599}{599}$ $\frac{601}{602}$ $\frac{603}{604}$ $\frac{605}{606}$ $\frac{607}{608}$ $\frac{609}{609}$ $\frac{611}{612}$ $\frac{613}{614}$ $\frac{615}{616}$ $\frac{617}{618}$ $\frac{619}{619}$ $\frac{621}{622}$ $\frac{623}{624}$ $\frac{625}{626}$ $\frac{627}{628}$ $\frac{629}{629}$ $\frac{631}{632}$ $\frac{633}{634}$ $\frac{635}{636}$ $\frac{637}{638}$ $\frac{639}{639}$ $\frac{641}{642}$ $\frac{643}{644}$ $\frac{645}{646}$ $\frac{647}{648}$ $\frac{649}{649}$ $\frac{651}{652}$ $\frac{653}{654}$ $\frac{655}{656}$ $\frac{657}{658}$ $\frac{659}{659}$ $\frac{661}{662}$ $\frac{663}{664}$ $\frac{665}{666}$ $\frac{667}{668}$ $\frac{669}{669}$ $\frac{671}{672}$ $\frac{673}{674}$ $\frac{675}{676}$ $\frac{677}{678}$ $\frac{679}{679}$ $\frac{681}{682}$ $\frac{683}{684}$ $\frac{685}{686}$ $\frac{687}{688}$ $\frac{689}{689}$ $\frac{691}{692}$ $\frac{693}{694}$ $\frac{695}{695}$ $\frac{697}{698}$ $\frac{699}{699}$ $\frac{701}{702}$ $\frac{703}{704}$ $\frac{705}{706}$ $\frac{707}{708}$ $\frac{709}{709}$ $\frac{711}{712}$ $\frac{713}{714}$ $\frac{715}{716}$ $\frac{717}{718}$ $\frac{719}{719}$ $\frac{721}{722}$ $\frac{723}{724}$ $\frac{725}{726}$ $\frac{727}{728}$ $\frac{729}{729}$ $\frac{731}{732}$ $\frac{733}{734}$ $\frac{735}{736}$ $\frac{737}{738}$ $\frac{739}{739}$ $\frac{741}{742}$ $\frac{743}{744}$ $\frac{745}{746}$ $\frac{747}{748}$ $\frac{749}{749}$ $\frac{751}{752}$ $\frac{753}{754}$ $\frac{755}{756}$ $\frac{757}{758}$ $\frac{759}{759}$ $\frac{761}{762}$ $\frac{763}{764}$ $\frac{765}{766}$ $\frac{767}{768}$ $\frac{769}{769}$ $\frac{771}{772}$ $\frac{773}{774}$ $\frac{775}{776}$ $\frac{777}{778}$ $\frac{779}{779}$ $\frac{781}{782}$ $\frac{783}{784}$ $\frac{785}{786}$ $\frac{787}{788}$ $\frac{789}{789}$ $\frac{791}{792}$ $\frac{793}{794}$ $\frac{795}{795}$ $\frac{797}{798}$ $\frac{799}{799}$ $\frac{801}{802}$ $\frac{803}{804}$ $\frac{805}{806}$ $\frac{807}{808}$ $\frac{809}{809}$ $\frac{811}{812}$ $\frac{813}{814}$ $\frac{815}{816}$ $\frac{817}{818}$ $\frac{819}{819}$ $\frac{821}{822}$ $\frac{823}{824}$ $\frac{825}{826}$ $\frac{827}{828}$ $\frac{829}{829}$ $\frac{831}{832}$ $\frac{833}{834}$ $\frac{835}{836}$ $\frac{837}{838}$ $\frac{839}{839}$ $\frac{841}{842}$ $\frac{843}{844}$ $\frac{845}{846}$ $\frac{847}{848}$ $\frac{849}{849}$ $\frac{851}{852}$ $\frac{853}{854}$ $\frac{855}{856}$ $\frac{857}{858}$ $\frac{859}{859}$ $\frac{861}{862}$ $\frac{863}{864}$ $\frac{865}{866}$ $\frac{867}{868}$ $\frac{869}{869}$ $\frac{871}{872}$ $\frac{873}{874}$ $\frac{875}{876}$ $\frac{877}{878}$ $\frac{879}{879}$ $\frac{881}{882}$ $\frac{883}{884}$ $\frac{885}{886}$ $\frac{887}{888}$ $\frac{889}{889}$ $\frac{891}{892}$ $\frac{893}{894}$ $\frac{895}{895}$ $\frac{897}{898}$ $\frac{899}{899}$ $\frac{901}{902}$ $\frac{903}{904}$ $\frac{905}{906}$ $\frac{907}{908}$ $\frac{909}{909}$ $\frac{911}{912}$ $\frac{913}{914}$ $\frac{915}{916}$ $\frac{917}{918}$ $\frac{919}{919}$ $\frac{921}{922}$ $\frac{923}{924}$ $\frac{925}{926}$ $\frac{927}{928}$ $\frac{929}{929}$ $\frac{931}{932}$ $\frac{933}{934}$ $\frac{935}{936}$ $\frac{937}{938}$ $\frac{939}{939}$ $\frac{941}{942}$ $\frac{943}{944}$ $\frac{945}{946}$ $\frac{947}{948}$ $\frac{949}{949}$ $\frac{951}{952}$ $\frac{953}{954}$ $\frac{955}{956}$ $\frac{957}{958}$ $\frac{959}{959}$ $\frac{961}{962}$ $\frac{963}{964}$ $\frac{965}{966}$ $\frac{967}{968}$ $\frac{969}{969}$ $\frac{971}{972}$ $\frac{973}{974}$ $\frac{975}{976}$ $\frac{977}{978}$ $\frac{979}{979}$ $\frac{981}{982}$ $\frac{983}{984}$ $\frac{985}{986}$ $\frac{987}{988}$ $\frac{989}{989}$ $\frac{991}{992}$ $\frac{993}{994}$ $\frac{995}{995}$ $\frac{997}{998}$ $\frac{999}{999}$ $\frac{1001}{1002}$ $\frac{1003}{1004}$ $\frac{1005}{1006}$ $\frac{1007}{1008}$ $\frac{1009}{1009}$ $\frac{1011}{1012}$ $\frac{1013}{1014}$ $\frac{1015}{1016}$ $\frac{1017}{1018}$ $\frac{1019}{1019}$ $\frac{1021}{1022}$ $\frac{1023}{1024}$ $\frac{1025}{1026}$ $\frac{1027}{1028}$ $\frac{1029}{1029}$ $\frac{1031}{1032}$ $\frac{1033}{1034}$ $\frac{1035}{1036}$ $\frac{1037}{1038}$ $\frac{1039}{1039}$ $\frac{1041}{1042}$ $\frac{1043}{1044}$ $\frac{1045}{1046}$ $\frac{1047}{1048}$ $\frac{1049}{1049}$ $\frac{1051}{1052}$ $\frac{1053}{1054}$ $\frac{1055}{1056}$ $\frac{1057}{1058}$ $\frac{1059}{1059}$ $\frac{1061}{1062}$ $\frac{1063}{1064}$ $\frac{1065}{1066}$ $\frac{1067}{1068}$ $\frac{1069}{1069}$ $\frac{1071}{1072}$ $\frac{1073}{1074}$ $\frac{1075}{1076}$ $\frac{1077}{1078}$ $\frac{1079}{1079}$ $\frac{1081}{1082}$ $\frac{1083}{1084}$ $\frac{1085}{1086}$ $\frac{1087}{1088}$ $\frac{1089}{1089}$ $\frac{1091}{1092}$ $\frac{1093}{1094}$ $\frac{1095}{1095}$ $\frac{1097}{1098}$ $\frac{1099}{1099}$ $\frac{1101}{1102}$ $\frac{1103}{1104}$ $\frac{1105}{1106}$ $\frac{1107}{1108}$ $\frac{1109}{1109}$ $\frac{1111}{1112}$ $\frac{1113}{1114}$ $\frac{1115}{1116}$ $\frac{1117}{1118}$ $\frac{1119}{1119}$ $\frac{1121}{1122}$ $\frac{1123}{1124}$ $\frac{1125}{1126}$ $\frac{1127}{1128}$ $\frac{1129}{1129}$ $\frac{1131}{1132}$ $\frac{1133}{1134}$ $\frac{1135}{1136}$ $\frac{1137}{1138}$ $\frac{1139}{1139}$ $\frac{1141}{1142}$ $\frac{1143}{1144}$ $\frac{1145}{1146}$ $\frac{1147}{1148}$ $\frac{1149}{1149}$ $\frac{1151}{1152}$ $\frac{1153}{1154}$ $\frac{1155}{1156}$ $\frac{1157}{1158}$ $\frac{1159}{1159}$ $\frac{1161}{1162}$ $\frac{1163}{1164}$ $\frac{1165}{1166}$ $\frac{1167}{1168}$ $\frac{1169}{1169}$ $\frac{1171}{1172}$ $\frac{1173}{1174}$ $\frac{1175}{1176}$ $\frac{1177}{1178}$ $\frac{1179}{1179}$ $\frac{1181}{1182}$ $\frac{1183}{1184}$ $\frac{1185}{1186}$ $\frac{1187}{1188}$ $\frac{1189}{1189}$ $\frac{1191}{1192}$ $\frac{1193}{1194}$ $\frac{1195}{1195}$ $\frac{1197}{1198}$ $\frac{1199}{1199}$ $\frac{1201}{1202}$ $\frac{1203}{1204}$ $\frac{1205}{1206}$ $\frac{1207}{1208}$ $\frac{1209}{1209}$ $\frac{1211}{1212}$ $\frac{1213}{1214}$ $\frac{1215}{1216}$ $\frac{1217}{1218}$ $\frac{1219}{1219}$ $\frac{1221}{1222}$ $\frac{1223}{1224}$ $\frac{1225}{1226}$ $\frac{1227}{1228}$ $\frac{1229}{1229}$ $\frac{1231}{1232}$ $\frac{1233}{1234}$ $\frac{1235}{1236}$ $\frac{1237}{1238}$ $\frac{1239}{1239}$ $\frac{1241}{1242}$ $\frac{1243}{1244}$ $\frac{1245}{1246}$ $\frac{1247}{1248}$ $\frac{1249}{1249}$ $\frac{1251}{1252}$ $\frac{1253}{1254}$ $\frac{1255}{1256}$ $\frac{1257}{1258}$ $\frac{1259}{1259}$ $\frac{1261}{1262}$ $\frac{1263}{1264}$ $\frac{1265}{1266}$ $\frac{1267}{1268}$ $\frac{1269}{1269}$ $\frac{1271}{1272}$ $\frac{1273}{1274}$ $\frac{1275}{1276}$ $\frac{1277}{1278}$ $\frac{1279}{1279}$ $\frac{1281}{1282}$ $\frac{1283}{1284}$ $\frac{1285}{1286}$ $\frac{1287}{1288}$ $\frac{1289}{1289}$ $\frac{1291}{1292}$ $\frac{1293}{1294}$ $\frac{1295}{1295}$ $\frac{1297}{1298}$ $\frac{1299}{1299}$ $\frac{1301}{1302}$ $\frac{1303}{1304}$ $\frac{1305}{1306}$ $\frac{1307}{1308}$ $\frac{1309}{1309}$ $\frac{1311}{1312}$ $\frac{1313}{1314}$ $\frac{1315}{1316}$ $\frac{1317}{1318}$ $\frac{1319}{1319}$ $\frac{1321}{1322}$ \frac

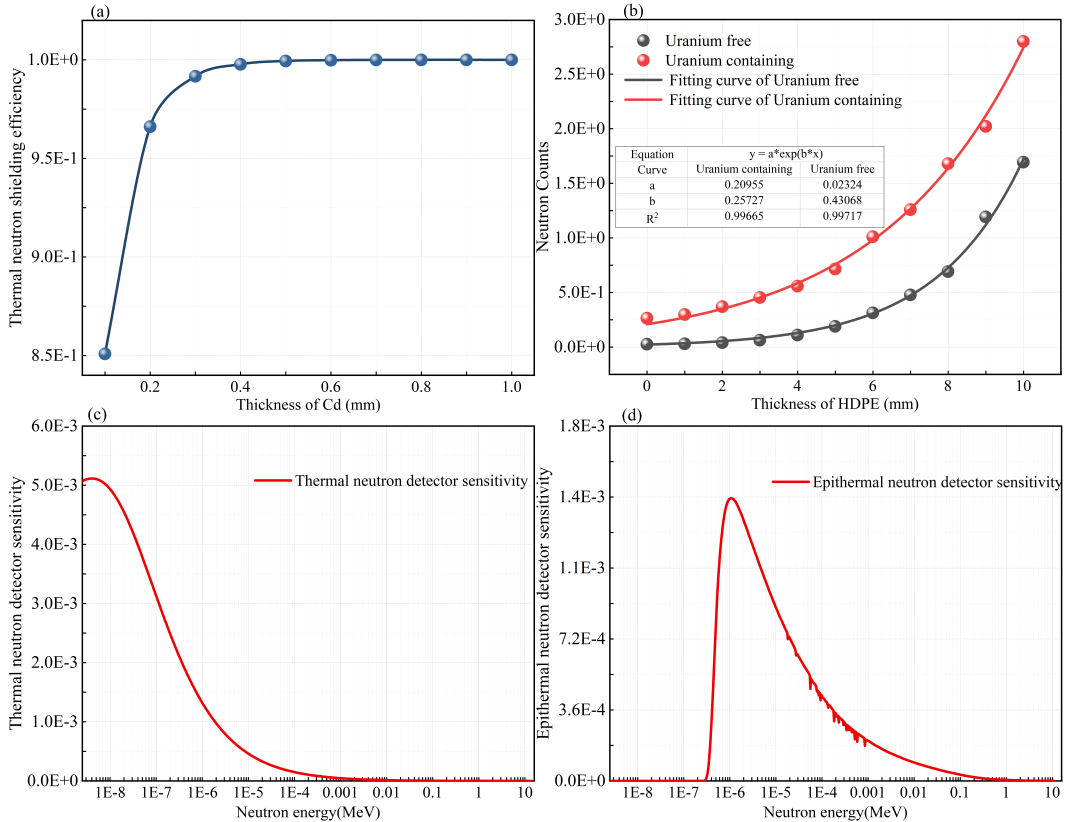


Fig. 3. (a) Cd metal thermal neutron shielding efficiency (b) HDPE thickness effect on epithermal neutron counting (c) Sensitivities of the ${}^3\text{He}$ detector (d) Sensitivities of the Epithermal neutron detector

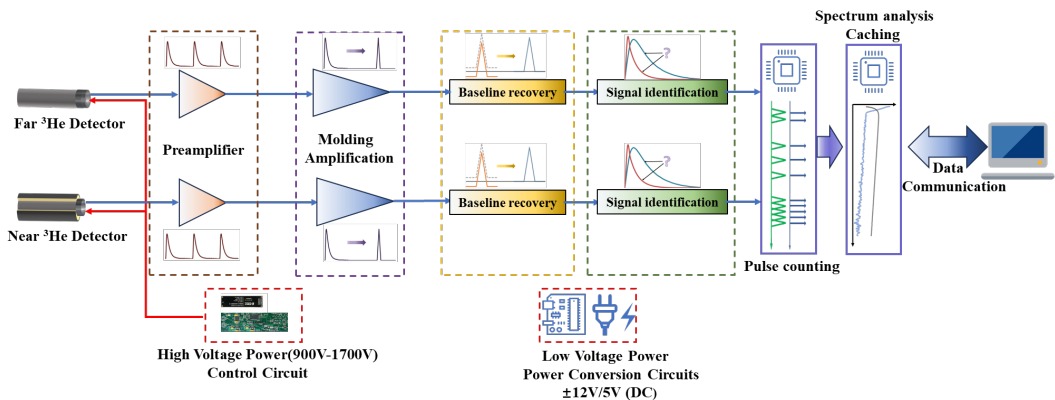


Fig. 4. Block diagram of dual-energy neutron time-spectrum measurement circuit structure

194 A digital FPGA chip (the radiation-resistant M2S010 from
 195 ACTEL) was selected as the core component to enable pulse
 196 counting for both epithermal and thermal neutrons, while also
 197 generating the corresponding time spectrum curves. Upon re-
 198 ceiving a synchronized measurement signal from the pulsed
 199 neutron generator, the FPGA starts counting pulse signals
 200 from the epithermal and thermal neutron detectors. The
 201 counts for both detectors are accumulated using a fine time-
 202 channel width of $2\ \mu\text{s}$, thus achieving precise dual-energy
 203 neutron time spectrum acquisition. The system simultane-

204 ously collects neutron energy and time spectra. By analyzing
 205 the shape of the neutron energy spectrum curve, a threshold
 206 is set for the countable neutron pulses, which ensures that
 207 the time spectrum only includes valid neutron pulses, exclud-
 208 ing noise and preventing the loss of effective neutron counts.
 209 This method ensures high accuracy in both the neutron en-
 210 ergy spectrum and the time spectrum measurements. When
 211 traditional logging systems based on analog signals are ap-
 212 plied to uranium logging, the presence of numerous analog
 213 components such as resistors, capacitors, and operational am-

214 plifiers makes them highly susceptible to temperature fluctu-
 215 ations in downhole environments. This leads to significant
 216 temperature drift, which increases the complexity of subse-
 217 quent spectral interpretation. In contrast, using a high-speed
 218 digital measurement system with key components such as
 219 high-speed A/D converters, FPGA, and DSP mitigates these
 220 issues. In this system, radiation pulse signals output by the
 221 detector are amplified and directly sampled in full pulse form
 222 by a high-speed A/D converter (with a sampling rate of 60
 223 MHz and a precision of 12 bits/1V). This approach captures
 224 the entire pulse waveform rather than just the peak value, as
 225 done in traditional systems. With the FPGAs internal pro-
 226 grammable digital circuits, algorithms like digital filtering
 227 and pulse shaping (using a dynamic trapezoidal shaping al-
 228 gorithm with adjustable parameters) are implemented. This
 229 allows for peak extraction, identification and separation of
 230 pile-up pulses, and generation of the energy spectrum curve.
 231 More complex tasks, such as dynamic temperature correction
 232 of pulse amplitudes and communication processing, are han-
 233 dled by the DSP. The designed digital measurement system
 234 includes a detector, preamplifier circuit, signal conditioning
 235 circuit, high-speed A/D converter, FPGA, and DSP. The in-
 236 fluence of power noise ripple and other electronic interference
 237 on the energy spectrum is controlled to $\leq 5\text{mV}/1\text{V}$, meaning
 238 that for a 1024 channels energy spectrum, noise contributes to
 239 no more than 5 channels.

240 D. Pulse Fast Shaping Neutron Time Spectrum

241 In the dual-neutron time spectrum detection system, a key
 242 challenge arises due to the high neutron count rate detected by
 243 neutron detectors immediately after the neutron pulse is emit-
 244 ted by the neutron source. This can cause significant pulse
 245 pile-up, particularly when using standard charge-sensitive
 246 preamplifier circuits paired with ^3He proportional counters,
 247 which have prolonged tail times on the signal decay. This
 248 pile-up effect often leads to saturation in the counting rate.
 249 To address this issue, a charge-sensitive preamplifier circuit
 250 based on narrow pulse shaping was designed for the neu-
 251 tron detector, significantly improving the pulse throughput
 252 of neutron signals. Additionally, the electronics system in-
 253 corporates full-pulse high-speed sampling technology, where
 254 the raw input pulse signals are directly sampled by a high-
 255 speed ADC, providing a complete waveform of the radiation
 256 pulse. The programmable digital circuits inside the FPGA
 257 implement triangular shaping algorithms, enabling the devel-
 258 opment of a dual-neutron time spectrum measurement sys-
 259 tem for PFNUL under high count rates. This narrow pulse
 260 shaping technique allows the processing of wider detector
 261 pulses into narrower pulses, facilitating counting measure-
 262 ment at high pulse throughputs [30–32]. The shaped pulse
 263 width is adjustable, and the experimental results, as shown
 264 in the Fig. 5a, demonstrate a reduction in signal pulse width
 265 from $1\text{ }\mu\text{s}$ to 300 ns . This enhancement increases the pulse
 266 processing capability of the electronics system from 100k to
 267 over 330k, ensuring the validity of the count measurements
 268 under high count rate conditions. After being processed by

269 the anti-saturation neutron detection system, the time spec-
 270 tra before and after fast shaping were obtained in the logging
 271 model for practical testing, as shown in Fig. 5b.

272 Additionally, the project conducted research on the time
 273 spectrum variation patterns of epithermal and thermal neu-
 274 trons under high count rates. In the software processing
 275 phase, a dead time correction algorithm was incorporated to
 276 account for the effects of pulse pile-up. This algorithm con-
 277 verts the observed pile-up count rate into the theoretical pulse
 278 count rate, thereby improving the accuracy of uranium quan-
 279 tification during the uranium logging process [33, 34].

280

III. LOGGING EXPERIMENTS

281 Using the independently developed PFNUL instrument
 282 UNL4, a series of experiments were conducted in five stan-
 283 dard model wells at the Nuclear Industry Aerial Survey and
 284 Remote Sensing Center. These wells consisted of cylindrical
 285 concrete models, identified as Nb4, Nu1, Nu2, and Nu3, with
 286 uranium concentrations of 0.000156%, 0.0280%, 0.0684%,
 287 and 0.0982%, respectively. The Nb4 model, with a uranium
 288 grade far below the detection limit, was defined as a pure
 289 sandstone model without uranium. Each cylindrical model
 290 measured 1.4m in diameter and 1.8m in height. The bore-
 291 hole diameter of the models was 90mm, and each model was
 292 topped with a 0.9m thick concrete cover and a 0.3m thick con-
 293 crete base. Beneath the base, an extended borehole of 2.6m
 294 in depth ensured that the size requirements for saturated ura-
 295 nium models were met. Another logging model, identified as
 296 PU, was a single cylindrical concrete structure with dimen-
 297 sions of 1.5m in diameter and 5.3m in height, along with an
 298 extended layer of 3m at the bottom. It contains two 90 cm
 299 sections with uranium contents of 87.1 ppm and 45.6 ppm, re-
 300 spectively. This setup allowed for continuous measurement of
 301 the uranium section when logging within the PU model. Sev-
 302 eral experiments were carried out in these five model wells,
 303 as outlined below, including comparisons between different
 304 neutron tubes:

305 (1)Experiment #1: Neutron Source Comparison

306 This experiment compared the performance of a probe with
 307 the domestically developed FH-G5DT neutron tube and a
 308 probe with the Russian ING-10-20-120 neutron tube in four
 309 uranium models, conducting point measurements.

310 (2)Experiment #2: Scale factor

311 Based on the time spectrum data, the E/T values of both
 312 neutron tubes were calculated at different uranium concentra-
 313 tions. A scale factor of E/T values and uranium concentra-
 314 tions was then derived through fitting.

315 (3)Experiment #3: Stability Test

316 In this experiment, short-term measurements were repeated
 317 10 times for 5 seconds each, and long-term measurements
 318 were repeated 9 times for 1 hour each in the same uranium
 319 concentration model, to assess stability.

320 (4)Experiment #4: Logging Speed Test

321 In the Nu3 model, neutron(E/T values) logging was con-
 322 ducted at speeds of 0.3 m/min, 0.5 m/min, 1 m/min ,1.5
 323 m/min, 2 m/min and 3 m/min to compare the results at dif-

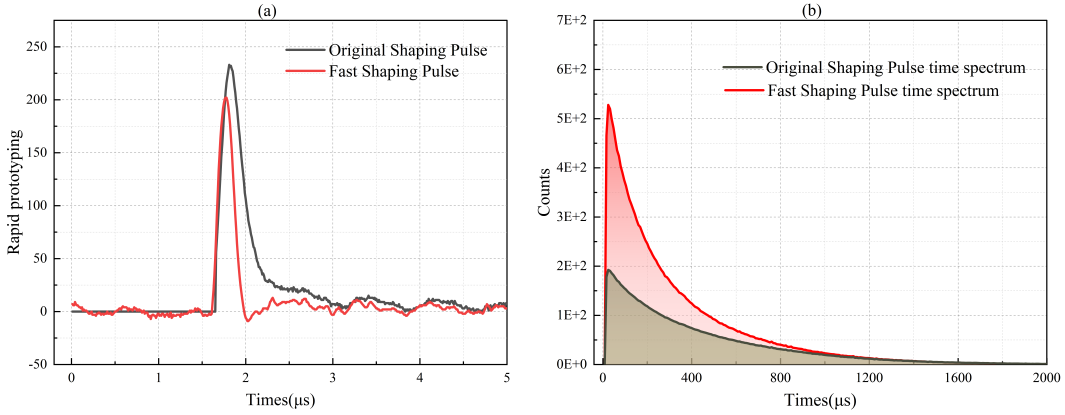


Fig. 5. (a)Pulsed Fast Shaping Measurement(b)Neutron time spectrum measurements in model wells before and after fast shaping

324 **ferent logging speeds, and gamma logging was conducted at**
 325 **speeds of 1 m/min, 2 m/min, 4 m/min, 6 m/min, 8 m/min and**
 326 **10 m/min.**

361 **of 20 emissions per second. In contrast, the FH-G5DT neu-**
 362 **tron tube, manufactured by Pan Hua Detection Co., employs**
 363 **a Penning ion source, which generates longer pulses (150 μs)**
 364 **and can emit up to 1000 times per second.**

327

IV. RESULTS AND DISCUSSION

328

A. Comparison of Different Neutron Sources

329 The time spectrum results obtained from testing different
 330 neutron tubes under four uranium ore models are illustrated
 331 in Fig. 6. In Fig. 6a, the results from the assembly of the Rus-
 332 sian ING-10-20-120 model neutron tube are presented, while
 333 Fig. 6b displays the results from the FH-G5DT model neu-
 334 tron tube. Due to variations in neutron tube manufacturing
 335 processes, the pulse widths for the neutron tubes were ap-
 336 propriately set to 10 μs and 250 μs during uranium ore mea-
 337 surements. The time spectrum results indicate a significant
 338 proliferation of epithermal neutrons with increasing uranium
 339 ore content.

340 From Fig. 6, it can be observed that the FH-G5DT neutron
 341 tube experiences a significant decline in the production of ep-
 342 iothermal neutrons at approximately 250 μs, leading to a very
 343 low counting rate of epithermal neutrons for times greater
 344 than 850 μs. At this point, statistical fluctuations substan-
 345 tially affect the data, prompting the selection of 250 μs to 850 μs as
 346 the effective neutron time window. Similarly, the ING-10-20-
 347 120 neutron tube shows a significant decrease in epithermal
 348 neutron production around 200 μs, with low counting rates
 349 for times exceeding 800 μs, where statistical fluctuations also
 350 play a considerable role. Consequently, the effective neu-
 351 tron time window for this tube is defined as 200 μs to 800
 352 μs. Within these time windows, epithermal and thermal neu-
 353 tron counts were calculated at various uranium content levels.
 354 The comparative results are illustrated in Fig. 7, which re-
 355 veals substantial differences in the counting rates of epither-
 356 mal and thermal neutrons between the two neutron tubes in
 357 same model. These discrepancies are primarily attributed to
 358 the different ion sources employed by the two neutron tubes.
 359 The Russian ING-10-20-120 neutron tube utilizes a vacuum
 360 arc ion source, producing short pulses (1 μs) with a maximum

366

B. Scale Factor

367 Based on the aforementioned conditions, the uranium
 368 quantification time windows for the two neutron tubes are
 369 200~800 μs and 250~850 μs, respectively. The E/T values
 370 were calculated according to the relevant data. Subsequently,
 371 a linear fitting of the relationship between the E/T values and
 372 uranium content was performed, as shown in Fig. 8. The cali-
 373 bration curves for the FH-G5DT and ING-10-20-120 neutron
 374 tubes were obtained, with calibration coefficients of 8.57 and
 375 4.24, respectively, and goodness-of-fit values (R^2) of 0.9998
 376 and 0.9996. Both neutron logging instruments demonstrated
 377 a strong linear calibration for the standard uranium ore model,
 378 with R^2 values exceeding 0.999. The results indicate that the
 379 neutron source, a key component of the neutron logging in-
 380 strument, significantly influences the calibration coefficient.
 381 Therefore, it is essential to recalibrate the instrument when
 382 the neutron source is changed, using a standard model bore-
 383 hole.

384

C. Instrument Stability

1. Short-term Stability Measurement

385 The UNL4 instrument conducted ten repeated measure-
 386 ments on the Nu3 model, using the RSD as a metric to as-
 387 sess the instrument's stability, with the calculation formula as
 388 shown in Eqs.1 [35, 36]. The results and RSD calculations
 389 are illustrated in Fig. 9(a~c). It can be observed that, across
 390 the ten repeated measurements, the counts of thermal neu-
 392 trons, epithermal neutrons, and the E/T values exhibit good
 393 repeatability, with RSD of 1.11%, 3.23%, and 3.16%, re-
 394 spectively.

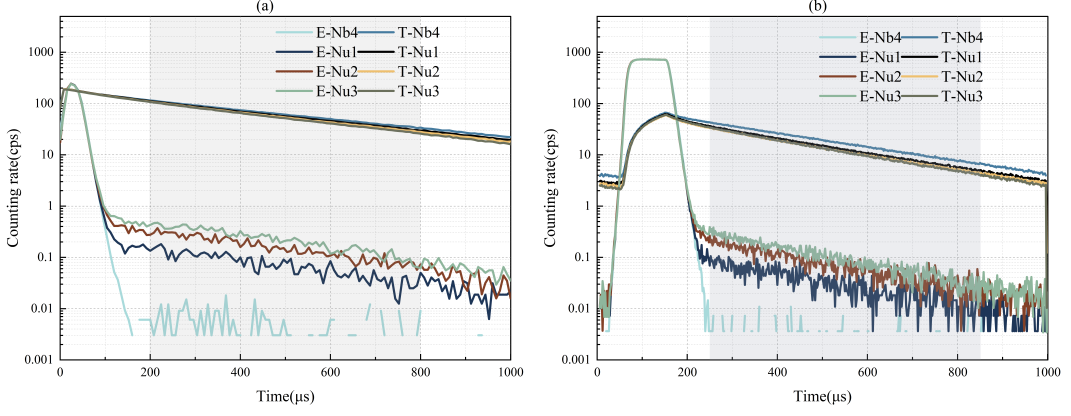


Fig. 6. (a) ING-10-20-120 neutron tube time spectra test results in Nu3 model (b) FH-G5DT neutron tube time spectra test results in Nu3 model

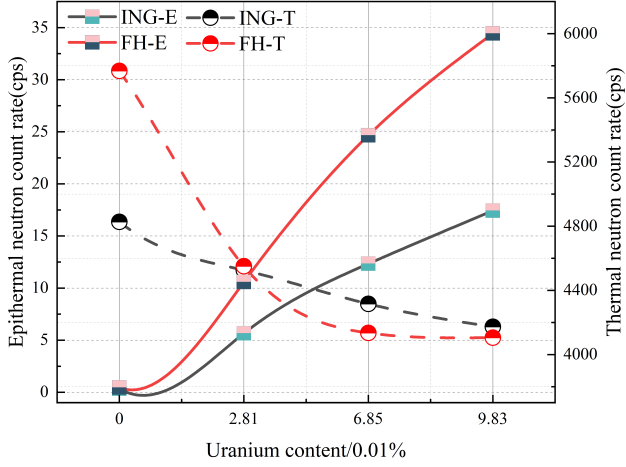


Fig. 7. The epithermal and thermal neutron counting results for the ING-10-20-120 and FH-G5DT neutron tubes

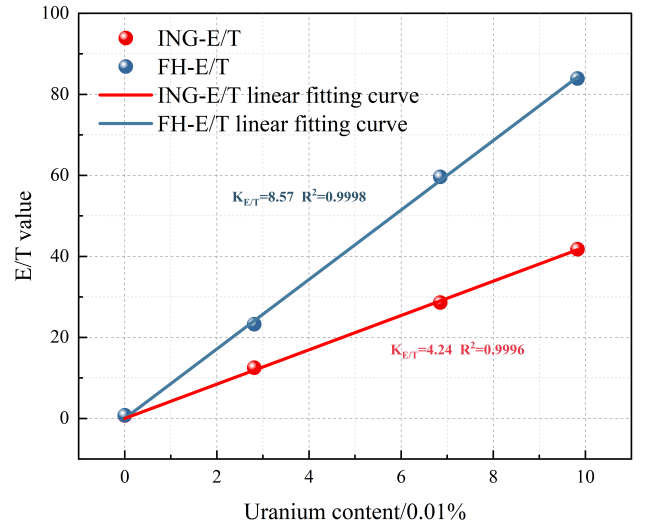


Fig. 8. E/T scale curves($K_{E/T}$) for ING-10-20-120 and FH-G5DT neutron tube

$$395 \quad RSD = \sqrt{\frac{\sum (count_i - \overline{count})^2}{n-1}} \quad (1)$$

396 Where $count_i$ represents the count for each data set, \overline{count}
 397 is the average count from multiple tests, n denotes the number
 398 of repeated measurements, and RSD is the result of the rela-
 399 tive standard deviation calculation, used to assess the stability
 400 of the instrument.

416 2. Long-term Stability Measurement

402 The UNL4 neutron logging instrument was used to conduct
 403 nine 1-hour long-term measurements on the Nu3 model. The
 404 data from each hour were normalized, and parameters were
 405 selected based on the aforementioned time window. The ef-
 406 fective thermal neutrons, epithermal neutrons, and E/T val-
 407 ues within the time window were then calculated. Stability

408 was analyzed using the RSD formula, with the specific data
 409 and calculation results shown in Fig. 9(e~f). As illustrated
 410 in the figures, the long-term stability of the neutron detection
 411 system shows that the long-term stability of thermal neutrons
 412 within the effective time window is 0.84%, that of epithermal
 413 neutrons is 1.49%, and that of the E/T values is 1.2%. These
 414 results demonstrate that the logging instrument exhibits ex-
 415 cellent stability.

416 D. Experiments at Different Logging Speeds

417 The UNL4 neutron logging instrument was used to con-
 418 duct measurements in the PU model well at the Remote Sens-
 419 ing Center, with neutron logging speeds set to 0.3 m/min, 0.5
 420 m/min, 1.0 m/min, 1.5 m/min, 2 m/min and 3 m/min and
 421 gamma logging speeds set to 1 m/min, 2 m/min, 4 m/min,
 422 6 m/min, 8 m/min and 10 m/min. The neutron logging curves

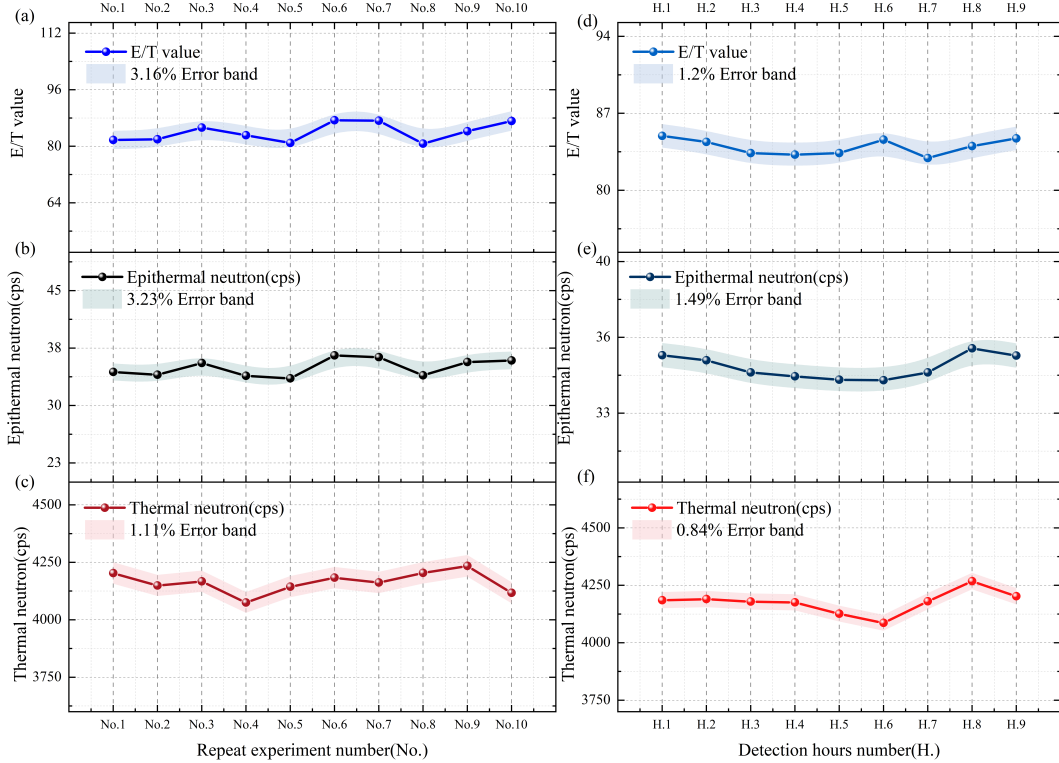


Fig. 9. (a-c) Short-time measurements of E/T values, Epithermal neutron counts rate and thermal neutron counts stability for neutron detection systems (e-f) Long-time measurements of E/T values, Epithermal neutron counts rate and thermal neutron counts rate stability for neutron detection systems

423 obtained at these five different speeds are shown in Fig. 10.
 424 It can be observed that at logging speeds ranging from 0.3
 425 to 3 m/min, the uranium-bearing sections of the formation
 426 (red) can be accurately identified. The quantitative uranium
 427 curve (green) demonstrates good consistency with the theo-
 428 retical curve (red). Table 3 lists the relative errors(*RD*) of the
 429 quantitative values for two uranium-bearing sections at differ-
 430 ent neutron logging speeds. The calculation formula for *RD*
 431 is shown in Eqs.2, where U_{Meas} represents the quantitative
 432 mean value of the ore section, and U_{Theor} is the theoretical
 433 value of uranium content. It can be observed that at logging
 434 speeds ranging from 0.3 to 3 m/min, the *RD* is below about
 435 10%. These findings indicate that the instrument can achieve
 436 stable quantification of uranium content at logging speeds of
 437 0.3 to 3 m/min. The direct uranium content scale based on
 438 gamma counting was carried out under the gamma logging
 439 experiment at different logging speeds, and the results are
 440 shown in Fig. 11. The results of the *RD* between the quantita-
 441 tive mean value and theoretical values of the two ore sections
 442 are shown in Table 4, the *RD* is below about 10%, with good
 443 stability and accuracy.

Table 3. Relative error of uranium content E/T values scale at different logging speeds

Uranium content	Neutron logging speeds(m/min)					
	0.3	0.5	1.0	1.5	2.0	3.0
87.1 ppm	<i>RD</i> -2.04%	0.81%	2.51%	-0.74%	0.70%	-10.45%
45.6 ppm	4.13%	-2.16%	12.55%	-4.91%	-0.66%	-20.37%

Table 4. Relative error of uranium content gamma counts scale at different logging speeds

Uranium content(ppm)	Gamma logging speeds(m/min)					
	1.0	2.0	4.0	6.0	8.0	10.0
87.1	<i>RD</i> 3.35%	-0.99%	1.29%	-1.37%	4.55%	-7.42%
45.6	2.63%	9.38%	2.15%	4.40%	5.95%	5.80%

E. Instrument Performance Parameters

446 In summary, after a series of optimizations and related ex-
 447 periments, the instrument has been proven to achieve interna-
 448 tionally leading standards for key technical indicators. De-
 449 tailed performance parameter comparisons are shown in Ta-
 450 ble 5. Due to the use of new pulse signal shaping hardware
 451 design in this instrument, the neutron signal pulse width has
 452 been effectively reduced, increasing the neutron detection ef-

$$444 \quad RD = \frac{U_{Meas} - U_{Theor}}{U_{Theor}} \times 100\% \quad (2)$$

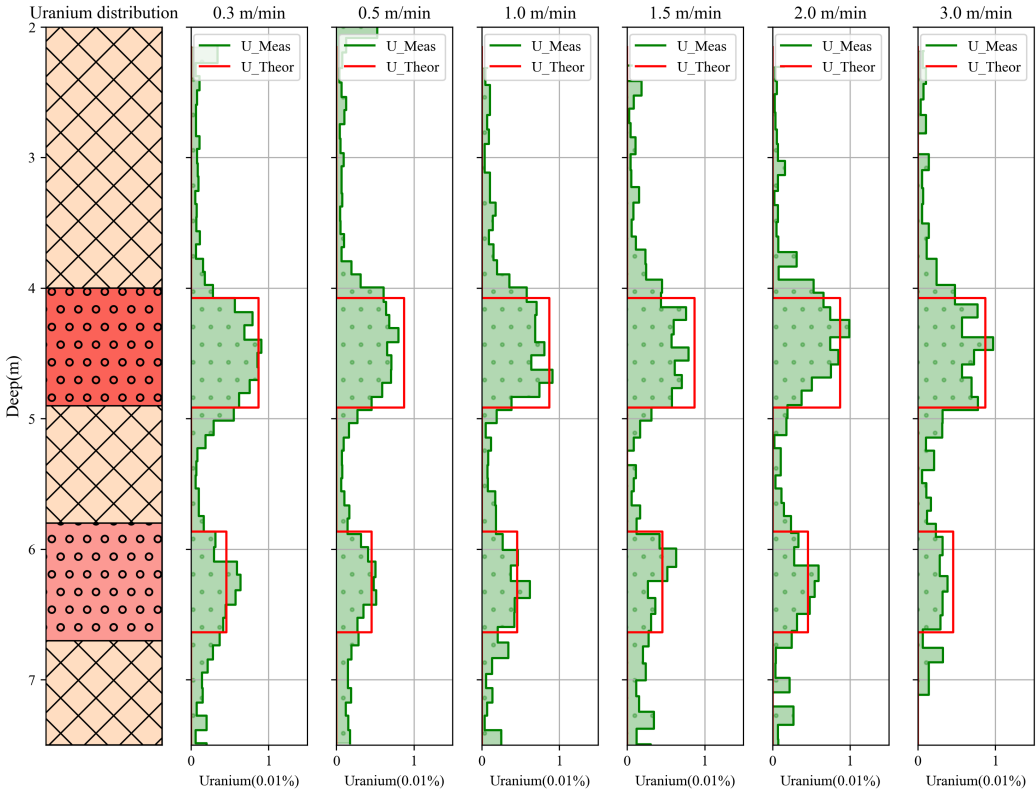


Fig. 10. E/T values logging quantification curves of uranium content in PU model at 0.3 m/min, 0.5 m/min, 1.0 m/min, 1.5 m/min, 2 m/min, 3 m/min logging speeds

453 ficiency. Coupled with a software dead-time correction algo-
 454 rithm [33], the time spectrum acquisition accuracy has been
 455 significantly improved, reducing the impact of dead time on
 456 uranium quantification. Additionally, the detector structure
 457 inside the probe has been optimized, and a uranium quan-
 458 tification algorithm based on the ratio of thermal neutrons to
 459 epithermal neutrons has been proposed [24]. This algorithm
 460 effectively reduces the impact of neutron source fluctuations,
 461 enabling accurate uranium content quantification. It can be
 462 observed that the neutron (E/T values) logging speed of the
 463 instrument has reached 3 m/min, the gamma logging speed
 464 has reached 10 m/min, and the detection limit is 45.6 ppm.
 465 The instrument operational lifespan exceeds 250 hours, and
 466 the neutron pulse width can be adjusted as needed. Compared
 467 to three other instruments, this instrument demonstrates a sig-
 468 nificant performance improvement.

469

V. CONCLUSION

470 In this study, we developed a new uranium fission prompt
 471 neutron logging instrument(UNL4), marking the first use of
 472 a domestically produced FH-G5DT neutron emitter, two ^3He
 473 proportional detectors, a lanthanum bromide (LaBr_3) gamma-
 474 ray detector, and a digital spectrometer. The system employs

475 high-speed ADC and FPGA technology to enable the rapid
 476 acquisition and transmission of dual neutron time spectra and
 477 gamma energy spectra. Additionally, a fast signal shaping
 478 method was proposed, which reduces the dead-time effect in
 479 ^3He detectors, thereby significantly improving neutron signal
 480 detection efficiency. Monte Carlo simulations were used to
 481 optimize the thickness of cadmium (Cd) and HDPE for ep-
 482 ithermal neutron detection. The optimal configuration was
 483 determined to be a Cd thickness of 1 mm and an HDPE thick-
 484 ness of 5 mm for the near ^3He detector, enabling efficient
 485 detection of epithermal neutrons. The far ^3He detector was
 486 employed to detect thermal neutrons, while the LaBr_3 detec-
 487 tor was used to detect gamma rays emitted by uranium ore it-
 488 self. Experimental results from standard borehole models with
 489 varying uranium content showed that the ratio of epithermal
 490 to thermal neutrons detected by instruments equipped with ei-
 491 ther the domestic FH-G5DT neutron tube or the Russian ING
 492 neutron tube exhibited a strong linear relationship with ura-
 493 nium content, with R^2 values of 0.9998 and 0.9996, respec-
 494 tively. This validated the effectiveness of the newly developed
 495 uranium fission prompt neutron logging instrument equipped
 496 with the domestic FH-G5DT neutron tube. Short-term test-
 497 ing indicated stability values of 1.11% for the thermal neutron
 498 count rate, 3.23% for the epithermal neutron count rate, and
 499 3.16% for the E/T values, long-term testing indicated stability
 500 values of 0.84% for the thermal neutron count rate, 1.49% for

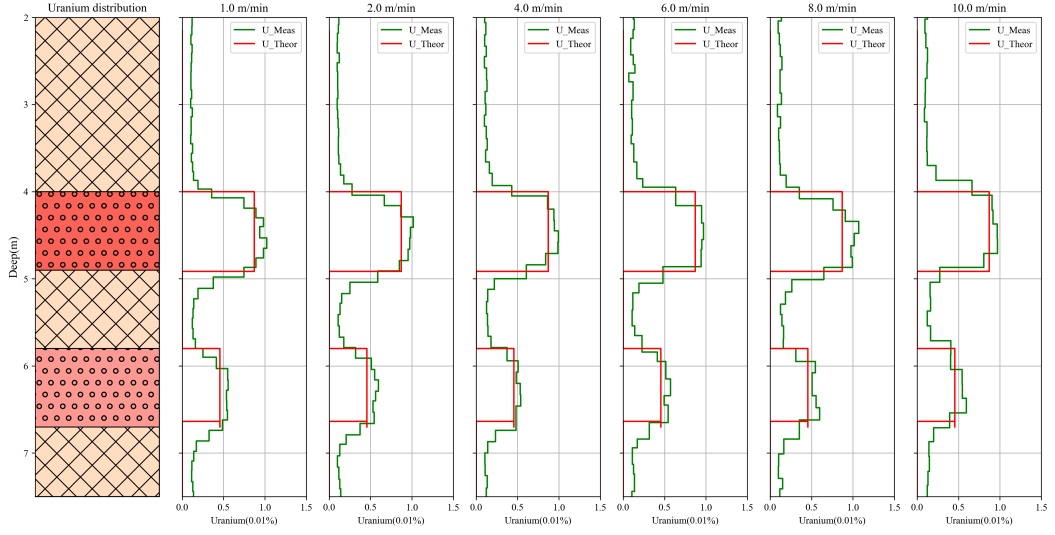


Fig. 11. Gamma logging quantification curves of uranium content in PU model at 1 m/min, 2 m/min, 4 m/min, 6 m/min, 8 m/min, 10 m/min logging speeds

Table 5. Comparison of Key Technical Indicators

Parameter	USA (PFN)[37]	Australia (APFN ⁺)[38]	Russian (ANHK-60)[39]	Logging Instrument UNL4(this paper)
Thin-layer and formation resolution	15 cm (0.5 feet)	15 cm (0.5 feet)	/	10 cm
Uranium detection limit(ppm)	500	50	50	45.6
Logging speed (orebody)	0.5 m/min	1 m/min (Neutron) 6 m/min (Gamma)	0.6 m/min	3 m/min (Neutron) 10 m/min (Gamma)
Neutron tube lifespan	/	/	150 h	≥ 250 h
Initial neutron tube output (n/s^{-1})	1×10^8	1×10^8	1.5×10^8	1.45×10^8
Pulsed neutron frequency	100 Hz	1000 Hz	20 Hz	1000 Hz (adjustable)
Detector type	³ He neutron detector (epithermal neutron) NaI gamma detector	³ He neutron detector (epithermal/thermal) LaBr ₃ gamma detector	³ He neutron detector (epithermal) NaI gamma detector	³ He neutron detector (epithermal/thermal) LaBr ₃ gamma detector

501 the epithermal neutron count rate, and 1.2% for the E/T val-
 502 ues, confirming the instrument's high stability. In addition,
 503 the instrument demonstrated good performance at neutron
 504 logging speeds of 0.3~3 m/min (E/T values) and gamma log-
 505 ging speeds of 1~10 m/min. By conducting measurements
 506 in two ore sections of the PU model with lithium contents of
 507 87.1 ppm and 45.6 ppm, the RD is less than about 10% in
 508 different neutron logging and gamma logging speeds, and de-
 509 tection limit reached 45.6 ppm. This instrument fills a critical
 510 gap in China uranium exploration neutron logging equipment
 511 and holds significant importance for the advancement of ura-
 512 nium exploration technology.

516 were performed by Hai-Tao Wang, Yan Zhang, Chi Liu, Jian-
 517 Qiang Xu, Li-Jiao Zhang, Zhi-Feng Liu, Xiong-Jie Zhang, Rui
 518 Chen, Qi Liu, Ren-Bo Wang, and Bin Tang. Hai-Tao Wang and
 519 Yan Zhang wrote the first draft of the manuscript, all authors
 520 commented on previous versions of the manuscript. All au-
 521 thors read and approved the final manuscript. Hai-Tao Wang
 522 and Yan Zhang contributed equally to this work and should
 523 be considered co-firstauthors.

513

VI. CONTRIBUTIONS STATEMENT

524

VII. CONFLICT OF INTEREST

514 All authors contributed to the study conception and de-
 515 sign. Material preparation, data collection and analysis

525

The authors declare that they have no competing interests.

VIII. DATA AVAILABILITY STATEMENT

527 The data that support the findings of this
 528 study are openly available in Science Data Bank
 529 at:<https://doi.org/10.57760/sciencedb.14086>

530 [1] W. Xing,A. Wang,Q. Yan et al., A study of Chinas uranium 531 resources security issues: Based on analysis of Chinas nu- 532 clear power development trend. *Ann. Nucl. Energy.* **110**,1156- 533 1164(2017).doi: [10.1016/j.anucene.2017.08.019](https://doi.org/10.1016/j.anucene.2017.08.019)

534 [2] CF. Mason, Uranium and nuclear power: The role 535 of exploration information in framing public pol- 536 icy. *Resour Energy Econ.* **36**(1),49-63(2014).doi: 537 [10.1016/j.reseneeco.2013.11.009](https://doi.org/10.1016/j.reseneeco.2013.11.009)

538 [3] H.R Zhang,Y. Zhang,W.X Hu et al.,Simulation study of 539 uranium content in uranium yellow cake using the active 540 multiplicity method. *Nucl. Tech.* **47**(02),020202(2024). doi: 541 [10.11889/j.0253-3219.2024.hjs.47.020202](https://doi.org/10.11889/j.0253-3219.2024.hjs.47.020202)

542 [4] B. Hou,J. Keeling,Z. Li. Paleovalley-related uranium de- 543 posits in Australia and China: A review of geological 544 and exploration models and methods. *Ore Geol. Rev.* **88**,201- 545 234(2017).doi:[10.1016/j.oregeorev.2017.05.005](https://doi.org/10.1016/j.oregeorev.2017.05.005)

546 [5] L.G. Howell,A. Frosch.GAMMARAY 547 WELLLOGGING. *Geophysics.* **4**(2),106- 548 114(1939).doi:[10.1190/1.1440486](https://doi.org/10.1190/1.1440486)

549 [6] C. Lin,Y.Q. Chen,Q.W. Zhang et al.,Calculation of U, Ra, Th 550 and K contents in uranium ore by multiple linear regression 551 method. *Nucl. Tech.* **6**,369-371(1991).

552 [7] B. Tang,Y.P. Wu,X.J. Zhang et al.,Direct uranium quantitative 553 detection in high precision γ -logging by 1.001 MeV 234mPa 554 γ -ray. *Nucl. Tech.* **35**(10),745-750(2012).

555 [8] J.H. Renken.Determination of the Probing Distance in 556 Pulsed-Neutron Uranium Logging Experiments. *Nucl. Sci. 557 Eng.* **63**(3),330-335(1977).doi:[10.13182/NSE77-A27044](https://doi.org/10.13182/NSE77-A27044)

558 [9] R.L. Caldwell, Nuclear Logging Methods, *Radioisotopes.* 559 **17**(4), 171-185 (1968).doi: [10.3769/radioisotopes.17.4_171](https://doi.org/10.3769/radioisotopes.17.4_171)

560 [10] W.W. Givens,W.R. Mills Jr.Logging technique for assaying 561 for uranium in earth formations. United States: N. p., 1979. 562 Web.<https://www.osti.gov/biblio/5327390>

563 [11] Z.F. Liu, C.L. Ding, R.Y. Wang et al., Current Status and Devel- 564 opment Trend Analysis of Neutron Logging in Uranium Mines 565 in China(IOP Publishing IOPscience, 2021).(Accessed Jan- 566 uary 19, 2024)<https://iopscience.iop.org/article/10.1088/1742-6596/1865/2/022006/meta>

567 [12] Y. Jin,F.L. Chen,X.Y. Chai et al.,Development 568 and Application of Nuclear Logging Technique. *At. Energy Sci. Technol.* **38**(S1),201-201(2004).doi: 569 [10.7538/yzk.2004.38.S1.0201](https://doi.org/10.7538/yzk.2004.38.S1.0201)

570 [13] X.G. Wang,D. Liu,F. Zhang.Development of pulsed 571 neutron uranium logging instrument. *Rev. Sci. In- 572 strum.* **86**(3),034501(2015).doi:[10.1063/1.4913660](https://doi.org/10.1063/1.4913660)

573 [14] C. Smith, Jeanneau, Philippe et al.,PFTNA logging instruments 574 and their contributions to in-situ elemental analysis of mineral 575 boreholes.TOS forum.(2015).doi: [10.1255/tosf.54](https://doi.org/10.1255/tosf.54)

576 [15] D. Chernikova,VL. Romodanov,AG. Belevitin AG et al., Ex- 577 perimental and numerical investigations of radiation charac- 578 teristics of Russian portable/compact pulsed neutron genera- 579 tors: ING-031, ING-07, ING-06 and ING-10-20-120. *Nucl. 580 Instrum. Methods Phys. Res., Sect. A.* **746**, 74-86(2014).doi: 581 [10.1016/j.nima.2014.01.061](https://doi.org/10.1016/j.nima.2014.01.061)

582 [16] K. Mikszuta-Michalik,R. Miklaszewski, Reconstruction of 583 neutron spectrum emitted by portable 14 MeV neutron gen- 584 erator by a combination of different methods. *Fusion Eng. 585 Des.* **199**,114129(2024).doi: [10.1016/j.fusengdes.2023.114129](https://doi.org/10.1016/j.fusengdes.2023.114129)

586 [17] Heikkinen DW. The rotating target neutron source II 587 facility: Operational summary. *Nucl. Instrum. Methods 588 Phys. Res., Sect. B.* **40-41**,1162-1164(1989).doi:[10.1016/0168-583X\(89\)90562-4](https://doi.org/10.1016/0168-583X(89)90562-4)

589 [18] J.H. Renken.Comparison of predicted signals from the 590 delayed fission neutron and prompt fission neutron 591 uranium logging methods. *J. Appl. Phys.* **49**(2),6153- 592 6159(1978).doi:[10.1063/1.324538](https://doi.org/10.1063/1.324538)

593 [19] R. W. Barnard,W. A. Stephenson,J. H. Weinlein et al., Ex- 594 periences with a PFN Uranium Logging System. *Trans. Nucl. 595 Sci.* **30**(2),1664 - 1667(1983). [10.1109/TNS.1983.4332610](https://doi.org/10.1109/TNS.1983.4332610)

596 [20] B. Tang, R.B. Wang, S.M. Zhou et al., Chinese patent 597 201310408465.6, 13 Sep.2013.

598 [21] B. Tang, R.B. Wang, S.M. Zhou et al., Chinese patent 599 201320592725.5, 2 Apr.2014.

600 [22] B. Tang, R.B. Wang, S.M. Zhou et al., Chinese patent 601 201310440359.6, 13 Sep.2013.

602 [23] Z.F. Liu,B. Tang,Z.H. Wei et al.,Correction Algorithm 603 of Epithermal Neutron Decay Time Spectrum for Ura- 604 nium Pulsed Neutron Logging. *For. Chem. Rev.* **1368-1376**(2022).www.forestchemicalsreview.com

605 [24] Y. Zhang,C. Liu,H.T. Wang et al., Prompt Fission Neutron Ura- 606 nium Logging(I): Direct Uranium Quantification Method The- 607 ory. *Nucl. Sci. Tech.*(Article in press).

608 [25] X.G. Wang,D. Liu,G.B. Wang.Optimization study of epither- 609 mal neutron detector in prompt fission neutron uranium log- 610 ging. *Nucl. Tech.* **36**(6),060401(2013).doi: [10.11889/j.0253-3219.2013.hjs.36.060401](https://doi.org/10.11889/j.0253-3219.2013.hjs.36.060401)

611 [26] H.Q. Zhang,B. Tang,H.X. Wu,Pulse amplitude ex- 612 traction in digital nuclear spectrometer system. *Nucl. 613 Tech.* **36**(5),050401(2013).doi: [10.11889/j.0253-3219.2013.hjs.36.050401](https://doi.org/10.11889/j.0253-3219.2013.hjs.36.050401)

614 [27] R. He,X.Y. Niu,Y.Wang et al.,Advances in nu- 615 clear detection and readout techniques. *NUCL. SCI. 616 TECH.* **34**(12),205(2024).doi: [10.1007/s41365-023-01359-0](https://doi.org/10.1007/s41365-023-01359-0)

617 [28] B. Tang,H.T. Wang,R. Cheng et al., Chinese patent 618 201810076976.5, 6 Aug.2018.

619 [29] D.W. Luo,H. Y. Wu,Z. H. Li et al.,Performance of digital 620 data acquisition system in gamma-ray spectroscopy. *Nucl. 621 Sci. Tech.* **32**(8),79(2021).doi: [10.1007/s41365-021-00917-8](https://doi.org/10.1007/s41365-021-00917-8)

622 [30] CH. Nowlin, Pulse Shaping for Nuclear Pulse Amplifiers. *Trans. Nucl. Sci.* **17**(1),226-241(1970).doi: 623 [10.1109/TNS.1970.4325584](https://doi.org/10.1109/TNS.1970.4325584)

624 [31] D. Yan,G. Dai,Q. Yuan et al., Research and Comparison of 625 Several Common Pulse Forming Algorithms. *Open Access 626 Libr.* **10**(3),1-11(2023).doi: [10.4236/ibalib.1109847](https://doi.org/10.4236/ibalib.1109847)

627 [32] VT. Jordanov,GF. Knoll,AC. Huber et al., Digital tech- 628 niques for real-time pulse shaping in radiation measure- 629 ments. *Nucl. Instrum. Methods Phys. Res., Sect. A.* **353**(1),261- 630 264(1994).doi:[10.1016/0168-9002\(94\)91652-7](https://doi.org/10.1016/0168-9002(94)91652-7)

638 [33] Y. Zhang,C. Liu,S.L. Liu et al.,Prompt Fission Neutron Uranium Logging(II): Dead-time effect of neutron time spec- 654 [37] R.W. Barnard, W.A. Stephenson, J.H. Weinlein
639 trum.Nucl. Sci. Tech.(Article in press). 655 et al., Experiences with a PFN Uranium Log-
640 656 ging System. IEEE Trans Nucl Sci.**30**(2),1664-
641 [34] J.W. Müller, Dead-time problems, Nucl. Instrum. 657 1667(1983).<https://doi.org/10.1109/TNS.1983.4332610>
642 Methods.**112**(1-2), 4757 (1973).doi: 658 [38] M. Horst,A.M. Smith, J. Ross et al., Advancements in Ex-
643 [10.1016/0029-554X\(73\)90773-8](https://doi.org/10.1016/0029-554X(73)90773-8) 659 ploration and In-Situ Recovery of Sedimentary-Hosted Uranium.
644 [35] Y. Zhang, B. Tang, W. Jia et al.,, Application of the 660 International Symposium on Uranium Raw Material
645 Monte Carlo Library Least-Squares (MCLLS) ap- 661 for the Nuclear Fuel Cycle: Exploration, Mining, Produc-
646 proach for chromium quantitative analysis in aqueous 662 tion, Supply and Demand, Economics and Environmental Is-
647 solution. Appl.Radiat.Isotopes. **150**, 3942 (2019).doi: 663 sues Presentations, (p. v). International Atomic Energy Agency
648 [10.1016/j.apradiso.2019.02.018](https://doi.org/10.1016/j.apradiso.2019.02.018) 664 (IAEA)(2014).
649 [36] Y. Zhang, W. Jia, R. Gardner, Q. Shan, D. Hei, 665 [39] V.G. Martynenko, A.R. Minosyants, S.N. Fedyanin, The
650 Study on the PGNAA measurement of heavy metals 666 Prospects for the Application of the New Generation Neutron
651 in aqueous solution by the Monte CarloLibrary Least- 667 Logging System Developed by Rusburmash Inc (Russian Fed-
652 Squares (MCLLS) approach. Appl.Radiat.Isotopes. **132**, 1317 668 eration) for Handling Geotechnical Issues at Sandstone-Hosted
653 (2018).doi: [10.1016/j.apradiso.2017.10.037](https://doi.org/10.1016/j.apradiso.2017.10.037) 669 Uranium Deposits. International Atomic Energy Agency
664 670 (IAEA): IAEA(2019).